# Finite-temperature analysis of a quasi-two-dimensional dipolar gas

Christopher Ticknor

Phys. Rev. A **85**, 033629 — Published 22 March 2012

DOI: 10.1103/PhysRevA.85.033629

# Finite temperature analysis of a quasi2D dipolar gas

Christopher Ticknor
*Theoretical Division, Los Alamos National Laboratory, Los Alamos, New Mexico 87545, USA*

We present finite temperature analysis of a quasi2D dipolar gas. To do this, we use the Hartree Fock Bogoliubov method within the Popov approximation. This formalism is a set of non-local equations containing the dipole-dipole interaction and the condensate and thermal correlation functions, which are solved self-consistently. We detail the numerical method used to implement the scheme. We present density profiles for a finite temperature dipolar gas in quasi2D, and compare these results to a gas with zero-range interactions. Additionally, we analyze the excitation spectrum and study the impact of the thermal exchange.

PACS numbers: 03.75Hh,67.85-d

## I. INTRODUCTION

Two hot topics in ultracold physics are two dimensional (2D) gases and dipolar gases. Reduced dimensionality enhances the quantum mechanical character of the system. In a homogeneous 2D system, quantum phase fluctuations are so strong that at finite temperature phase coherence cannot be established and condensation does not occur. There is, however, an intriguing phase transition called the Berezinskii-Kosterlitz-Thouless (BKT) transition [1] which occurs when the temperature is lowered and there is no longer enough thermal energy to unbind vortex and anti-vortex pairs. This binding of vortices reduces phase fluctuations so that quasi-long range order can form [2]. Interestingly, a trapped 2D gas can form a Bose Einstein condensate (BEC) at finite temperature [2, 3]. The BKT and BEC transition have been studied in trapped ultracold gases, first by observations of phase defects [4], direct observation of vortices[5], and then changes in the density profile due to the onset of superfluidity [6]. Additionally, universality has been observed near the BKT transition [7]. Successful methods which study such systems are Monte Carlo [8, 9], mean field [11, 12] and classical-field methods [13–15].

In dipolar systems the interactions are non-local and the possibility of creating strongly correlated gases are tantalizing, especially in quasi-2D (q2D) where zero point motion in the axial direction is included. For example, some studies have used Monte Carlo methods to study phase transitions such as crystallization [16]. This study included temperature as a variable and observed melting of the dipolar crystal. The BKT transition of a homogeneous dipolar gas has been studied with Monte Carlo methods to examine superfluid fraction and excitation spectra [17]. Other studies have looked at the structure of the dipolar gas and the impact of temperature on the phase of the gas [18, 19]. Such studies have focused on strongly interacting dipolar systems. However, the bulk of the work on q2D gases has been at zero temperature. For example, phonon instability [20] and anisotropic superfluidity [21] have been predicted.

Recently, chromium (Cr) and dysprosium (Dy) have been Bose condensed and exhibited strong dipolar effects [22, 23]. Additionally, progress towards a q2D dipolar gas has been made with a layered dipolar system for Cr atoms in a one dimensional optical lattice [24]. With such progress on dipolar gases, direct study of q2D dipolar systems has begun. An important question is how will dipolar interactions impact the quantum behavior of a q2D gas? The long range nature of the dipolar interaction may lead to interesting physics for the thermal system, especially relating the BKT transition and phase coherence. Additionally, little work studying the impact of temperature on q2D dipolar gases has been conducted for reasonable experimental parameters.

With an eye toward this unexplored physics and aiding experiments, we study the finite temperature physics of q2D trapped dipolar gases. We use the standard beyond mean-field method: the Hartree Fock Bogoliubov within the Popov approximation (HFBP) [25]. The HFBP has been successful in studying ultracold atoms, for example it has been used to explain the temperature dependence of collective excitations in a 3D BEC [26]. In the case of 3D dipolar gases, Ref. [27] used the HFBP to study temperature effects on the biconcave structure dipolar gases can have [28]. This study neglected the thermal exchange. Other recent work used mean field methods to study the stability of finite temperature dipolar gases [29].

The aim of this paper is two fold. First, we develop a numerical method to solve the non-local HFBP. This method includes the non-local interaction and exchange effects. We show in detail how the interaction and thermal exchange effects are included; it relies on a parallel implementation of the method. The method can also be applied to dipolar fermions. Second, we compare the contact gas and the dipolar gas with the HFBP. In the comparison of the two gases, we look at the condensate number as a function of temperature. We also articulate the role of thermal exchange in the gas by solving the system with and without thermal exchange. We compare the density profiles of the gas at various temperatures. We look at the excitation spectrum as a function of both temperature and total particle number. We also classify the lowest excitation modes. To the author's knowledge, these results are the first for a q2D trapped-finite temperature dipolar gas with thermal exchange effects.

## II. EQUATIONS OF MOTION

We study a quasi-2D dipolar system at finite temperature. To do this, we will employ the Hartree Fock Bogoliubov method within the Popov approximation with non-local interactions [25, 30]. The HFB breaks the second quantized bosonic field operator into a condensate and non-condensate (thermal) component: $\hat{\Psi} = [\sqrt{N_0}\phi_0(x) + \hat{\theta}(x)]$ where we have replaced $\hat{a}_0 \rightarrow \sqrt{N_0}$. Here $x$ represents all required coordinates, for the 2D case it will be $\vec{\rho}$. We will use the Bogoliubov transformation for the thermal part: $\hat{\theta}(x) = \sum_\alpha [u_\alpha(x)\hat{a}_\alpha e^{-i\omega_\alpha t} - v^*_\alpha(x)\hat{a}^*_\alpha e^{i\omega_\alpha t}]$ where $\hat{a}$ ($\hat{a}^*$) is the bosonic annihilation (creation) operator for a quasi-particle (hole). They obey the bosonic commutation relations: $[\hat{a}_\alpha, \hat{a}^*_\beta] = \delta_{\alpha\beta}$ and $[\hat{a}_\alpha, \hat{a}_\beta] = [\hat{a}^*_\alpha, \hat{a}^*_\beta] = 0$. To derive the equations of motion we start with the Heisenberg equation of motion with a non-local interaction [30]. We find for our system the modified non-local Gross Pitaevskii equation (GPE) is

$$\mu\phi_0(x) = \left(H_0 + \int dx' n(x')V\right)\phi_0(x) + \int dx'[\tilde{n}(x,x') - \tilde{m}(x,x')]V\phi_0(x'), \tag{1}$$

where $H_0$ is the kinetic energy and trapping potential. The interaction potential, $V(x-x')$, has been written as $V$ for simplicity. The total density, $n(x) = n_0(x) + \tilde{n}(x)$ is made up of condensate density and thermal density. The non-local correlation functions are: $n_0(x,x') = N_0\phi^*_0(x)\phi_0(x')$ and $n_0(x) = n_0(x,x)$; $\tilde{n}(x,x') = \langle\hat{\theta}^*(x)\theta(x')\rangle$ is the thermal correlation function and the local thermal density is $\tilde{n}(x) = \tilde{n}(x,x)$. $\tilde{m}(x,x') = \langle\hat{\theta}(x)\hat{\theta}(x')\rangle$ is the anomalous thermal correlation function, and in the Popov approximation is neglected. The quasi-particle wavefunctions are required to construct the thermal and anomalous correlation functions. At equilibrium, these wavefunctions can be found from a non-local Bogoliubov-de Gennes equation:

$$\begin{aligned}\omega_\alpha u_\alpha(x) = &\left(H_0 - \mu + \int dx' n(x')V\right)u_\alpha(x) + \int dx'[n_0(x,x') + \tilde{n}(x,x')]Vu_\alpha(x') \\ &+ \int dx'\tilde{m}(x,x')Vv_\alpha(x') - \int dx' m_0(x,x')Vv_\alpha(x') \\ -\omega_\alpha v_\alpha = &\left(H_0 - \mu + \int dx' n(x')V\right)v_\alpha(x) + \int dx'[n_0(x,x') + \tilde{n}(x,x')]Vv_\alpha(x') \\ &+ \int dx'\tilde{m}^*(x,x')Vu_\alpha(x') - \int dx' m^*_0(x,x')Vu_\alpha(x').\end{aligned} \tag{2}$$

The total number of atoms is $N = N_0 + \tilde{N}$ and $\tilde{N} = \int dx\tilde{n}(x)$. The normalization of the quasi-particle wavefunction is $1 = \int dx(|u_\alpha|^2 - |v_\alpha|^2)$. The anomalous condensate correlation function is $m_0(x,x') = N_0\phi(x)\phi(x')$. The thermal correlation functions are defined in terms of the quasi-particles:

$$\tilde{n}(x,x') = \sum_\alpha [u^*_\alpha(x')u_\alpha(x) + v_\alpha(x')v^*_\alpha(x)]\, N^\alpha_{be} + v_\alpha(x')v^*_\alpha(x) \tag{3}$$

$$\tilde{m}(x,x') = \sum_\alpha [u_\alpha(x')v^*_\alpha(x) + v^*_\alpha(x')u_\alpha(x)]\, N^\alpha_{be} + u_\alpha(x')v^*_\alpha(x), \tag{4}$$

where $N^\alpha_{be} = (Ze^{\hbar\omega_\alpha/kT} - 1)^{-1} = \langle\hat{a}^*_\alpha\hat{a}_\alpha\rangle$ where $k$ is Boltzmann's constant, $T$ is the temperature, and $Z = 1 + 1/N_0$. This relation is simply the Bosonic occupation of thermal modes. These equations are consistent with Refs. [27], [30], and [31] when the appropriate simplification is made.

To make the discussion of Eqs. (1) and (2) simpler, we introduce a compact notation:

$$
\begin{aligned}
&(H_0 + D + \tilde{X} + \tilde{M})\phi_0 = \mu\phi_0, && (5)\\
&(H_0 - \mu + D + X)u_\alpha + Mv_\alpha = \omega_\alpha u_\alpha, && (6)\\
&(H_0 - \mu + D + X)v_\alpha + Mu_\alpha = -\omega_\alpha v_\alpha. &&
\end{aligned}
$$

The first term is the standard kinetic and potential energy, $H_0$. For the remaining interaction terms, we use the capital letters to indicate the inclusion of the $x'$ integral, so the direct interaction is $D = D_0 + \tilde{D}$ (condensate and thermal), and for example $D_0(x) = \int dx'[n_0(x')]V(x - x')$. The exchange interaction is $X = X_0 + \tilde{X}$ (condensate and thermal), and for example $\tilde{X}(x, x') = \int dx'[\tilde{n}(x, x')]V(x - x')$. Finally, the anomalous correlation function is $M = \tilde{M} - M_0$, and for example $M(x, x') = \int dx'[\tilde{m}(x, x') - m_0(x, x')]V(x - x')$. We will use the Popov approximation, which assumes $\tilde{M} = 0$, leading to $M = -X_0$ if $\phi_0$ is real. This approximation keeps the spectrum gapless.

We project out the condensate mode from the quasiparticles, as was done in Refs. [32, 33] which uses $Q = 1 - |0\rangle\langle 0|$ and $\langle x|0\rangle = \phi_0(x)$. The projection operator is applied to all operators that are not in $H_{GP} = H_0 - \mu + D + \tilde{X}$, such as $M_0$ and $X_0$, and for example, $M_0 \to QM_0Q$. This projection method keeps the spectrum gapless.

## III. THE INTERACTION

We are interested in the q2D dipolar system assuming no axis of symmetry, so we take the dipole moment to be $\vec{d} = d(\hat{z}\cos(\alpha) + \hat{x}\sin(\alpha))$, and we assume harmonic confinement and that $\omega_z \gg \omega_\rho$ where the $\omega_i$ are the trapping frequencies ( $\omega_x = \omega_y = \omega_\rho$). This allows us to assume only one transverse mode is occupied in the $z$ direction. We can then evaluate the interaction by factoring the wavefunction as $\psi(\vec{r}) = \chi_0(z)\psi(\vec{\rho})$, where $\psi$ is either $\phi_0$, $u_\alpha$, or $u_\alpha$ and $\chi_0$ is eigenstate of $H_0$ in the $z$ direction. We are then able to integrate out $z$, and obtain an effective interaction. We will also consider a contact interaction. The interaction we use is:

$$
V(\vec{\rho}) = g\delta(\vec{\rho}) + g_d V_{dd}(\vec{\rho}), \tag{7}
$$

where $g = \sqrt{8\pi}\hbar^2 a_s/ml_z$ is the strength of the contact interaction, $a_s$ is s-wave the scattering length ($a_s \ll l_z$), $l_z = \sqrt{\hbar/m\omega_z}$ is the axial harmonic oscillator length, $g_d = d^2/\sqrt{2\pi}l_z$ and $d$ is the dipole moment of the particles. This interaction leads to the dipolar length scale: $l_d = md^2/\hbar^2$. In practice, we rescale the equations of motion into oscillator units, where the units of energy and length are: $\hbar\omega_\rho$ and $l_\rho = \sqrt{\hbar/m\omega_\rho}$. After this rescaling, the dipolar interaction strength becomes $g_d = l_d/(l_z\sqrt{2\pi})$. Finally, the dipolar interaction in q2D is:

$$
\begin{aligned}
V_{dd}(\vec{\rho} - \vec{\rho}') &= \int dz\chi_0^2(z)\int dz'\chi_0^2(z')V_d^{3D}(\vec{r} - \vec{r}') && (8)\\
V_{dd}^{3D}(\vec{r}) &= d^2(1 - 3(\hat{d}\cdot\hat{r})^2)/r^3. &&
\end{aligned}
$$

The interaction is evaluated in momentum space. As an example, the direct interaction is:

$$
\begin{aligned}
D(\vec{\rho}) &= \mathcal{F}^{-1}\left[n(\vec{k})\tilde{V}\left(\vec{k}\right)\right] && (9)\\
\tilde{V}(\vec{k}) &= g_d\frac{4\pi}{3}F\left(\frac{\vec{k}l_z}{\sqrt{2}}\right), &&
\end{aligned}
$$

where $\mathcal{F}$ is the Fourier transform operator and $n(\vec{k}) = \mathcal{F}[n(\vec{\rho})]$. $\tilde{V}_k$ is the momentum representation of the interaction. The function $F(\vec{k})$ is the $k$-space dipolar interaction for the q2D geometry. It has two contributions coming from polarization perpendicular to and in the direction of the dipole tilt, $F(\vec{k}) = \cos^2(\alpha)F_\perp(\vec{k}) + \sin^2(\alpha)F_\parallel(\vec{k})$ where $\alpha$ is the angle between $\hat{z}$ and the polarization vector $\hat{d}$. Its contributions are $F_\parallel(\vec{k}) = -1 + 3\sqrt{\pi}(k_d^2/k)e^{k^2}\mathrm{erfc}(k)$, where $\vec{k}_d$ is the wave vector along the polarization direction in the x-y plane, erfc is the complementary error function and $F_\perp(\vec{k}) = 2 - 3\sqrt{\pi}ke^{k^2}\mathrm{erfc}(k)$ [20, 21, 34].

To evaluate the exchange interaction, we use a simple, yet memory intensive, solution: we explicitly construct the interaction on the same space-space grid as the correlation functions. We put $n(\vec{\rho}, \vec{\rho}')$ on a grid specified by the indices $s$ and $t$, representing $\vec{\rho}$ and $\vec{\rho}'$. Each grid has $n_s$ spatial points, and a correlation function has $n_s^2$ grid points.

To evaluate the interaction, we work in momentum space. The interaction on the space-space grid is:

$$
V_{st} = W_{sk}^T\tilde{V}_k W_{kt}. \tag{10}
$$

where $W_{ks}$ is the operator that transforms between space ($s$) and k-space ($k$) representation via the spectral basis set [35]. The operator takes the place of the Fourier operator in our algorithm. An important aspect of the method is that it regularizes the interaction and avoids the logarithmic divergence as $\vec{\rho} \to \vec{\rho}'$ encountered by directly evaluating Eq. (8) because $W_{kt}$ involves a projecting onto the Gauss-Hermite basis set [35]. Constructing the interaction involves the most costly step, requiring $n_s^3$ operations per node. This is performed only once for a set of interaction parameters ($l_z$ and $\alpha$) and basis set size.

We have constructed a parallel implementation of the method. We distribute the $s$ index ($\vec{\rho}$ grid) across the computing nodes ($p$); we will denote this distributed index as $s_p$. This way, each core handles only a fraction of the correlation functions and interaction. In the future, we will construct the interaction in the partial wave expansion: $V(\vec{\rho}) = \sum_m V_m(\rho, \phi)$. This expansion will be necessary to handle an interaction which depends on quantum numbers such as $n_z$ (confinement in $z$) or spin.

## IV. NUMERICAL IMPLEMENTATION

We solve Eqs. (5) and (6) by expanding the wavefunctions on the basis that diagonalizes $H_0$. We will focus on the harmonically trapped case where $H_0\chi_\alpha = \epsilon_\alpha\chi_\alpha$, $\int d\vec{\rho}\chi^*_\alpha(\vec{\rho})\chi_\beta(\vec{\rho}) = \delta_{\alpha\beta}$, and $\epsilon_\alpha = \hbar\omega_\rho(m_x + m_y + 1)$ where $m_\alpha$ is an integer. In a basis set, the evaluation of the direct interaction term, $D_{\alpha\beta}$, is straight forward: $\int d\vec{\rho}\chi_\alpha(\vec{\rho})[\int dx' V(\vec{\rho}-\vec{\rho}')n(\vec{\rho}')]\chi_\beta(\vec{\rho})$, where the quantity in the square brackets is the effective potential from the interaction. The more complicated terms are the non-local exchange terms, such as the thermal exchange: $\tilde{X}_{\alpha\beta}$ which is $\int d\vec{\rho}\chi^*_\alpha(\vec{\rho})\int d\vec{\rho}'\tilde{n}(\vec{\rho},\vec{\rho}')V(\vec{\rho}-\vec{\rho}')\chi_\beta(\vec{\rho}')$.

The non-local exchange term in the spectral basis is: $X_{\alpha\sigma} = U^T_{\alpha s}V_{st}n_{st}U_{t\sigma}$, where $U_{s\sigma}$ is the transformation between the spectral basis ($\sigma$) and space basis ($s$). The numerical procedure to evaluate this on node $p$ is: (1) $Y_{s_p t} = V_{s_p t}n_{s_p t}$, multiply the interaction and correlation function; (2) $h_{s_p\sigma} = Y_{s_p t}U_{t\sigma}$, project the $t$ spatial basis onto the $\sigma$ spectral basis; (3) $X^p_{\alpha\sigma} = \sum_{s_p} U^T_{s_p\alpha}h_{s_p\sigma}$, project $s_p$ spatial basis onto the $\alpha$ spectral basis; and (4) $X_{\alpha\sigma} = \sum_p X^p_{\alpha\sigma}$, collect and sum. In comparison, the direct terms are straight forward and evaluated in momentum space at each step. $\Phi_s = W_{sk}\tilde{V}_k W_{kt}n_t$, where $\Phi_s$ is the effective potential. Then we must project onto the basis: $D_{\alpha\sigma} = U^T_{\alpha s}\Phi_s U_{s\sigma}$, and this is done in parallel.

The procedure to find the full solution is: set temperature, $T$, and $N_0$ and pick a targeted value for the total number of particles in the system, $N_{target}$, and set $\tilde{n} = 0$ and $\tilde{m} = 0$:

1. Solve Eq. (1) for $\phi_0$ and $\mu$ (in basis set).
2. Construct condensate exchange term, $X_0$, with $n_0(\vec{\rho},\vec{\rho}')$ and put in basis set.
3. Solve Eq. (2) for $u_\alpha$ and $v_\alpha$.
4. Construct $\tilde{n}(\vec{\rho},\vec{\rho}')$ and $\tilde{m}(\vec{\rho},\vec{\rho}')$.
5. Use the semi-classical LDA to supplement the thermal tail (see below), which gives $\tilde{N}$ and therefore $N = N_0 + \tilde{N}$.
6. Construct thermal and anomalous exchange terms, $\tilde{X}$ and $\tilde{M}$ (if not using Popov approximation), and put in basis set representation.
7. Adjust $N_0$ to get the desired $N_{target}$ of atoms. We require N to be within 1% of $N_{target}$.
8. Go back to step 1 until self-consistency is reached. We converge the number of thermal atoms, so that $|\tilde{n}_i - \tilde{n}_{i-1}| < 5\cdot 10^{-5}$, when we are near enough $N_{target}$.

With the numerical method in hand, we are ready to proceed to the physical examples and the results.

The semi-classical, local density approximation (LDA) is very important for large $\vec{\rho}$ and high momentum states on the grid. At high temperature with a manageable grid size (much bigger than the condensate), we find that there can be a appreciable number of atoms outside of quadrature grid. For the large $\vec{\rho}$ contributions, the density is low enough that the analytic, non-interacting solution can be used to account for these off-grid particles. We integrate the analytic solution over a large region outside of the grid. We have tested that this does not impact the convergence of the end result. We include the impact of higher transverse modes in the same analytic manner on and off the grid. We also assume that these particles in the higher $z$ modes are non-interacting. This is reasonable, especially because symmetry prevents the first excited transverse mode from colliding with the condensate with $m = 0$ symmetry. Additionally, a noticable number of thermal particles are in momentum states beyond calculated quantum spectrum [36, 37]. To include these thermal atoms we use the method from Ref. [27].

## V. PHYSICAL EXAMPLES

We will study Cr and Dy atoms. These atoms have been Bose condensed and shown to exhibit strong dipolar effects [22, 23]. The first example we choose is: $2\cdot 10^3$ Cr atoms with $l_d = 45a_0$ where $a_0$ is the Bohr radius. This gives $g_d = 0.0028$ and $g = 0$ in trap units. Additionally, we pick $l_z/l_\rho = 0.1$, this is from using $(\omega_\rho,\omega_z){=}2\pi$ (16,1600) Hz. We have found that our numerical procedure using 465 basis states with an energy cut of $30\hbar\omega_\rho$ converges. To compare this to a contact gas, we match the chemical potential at zero temperature by varying $g$. We will only consider $\alpha = 0$ here, that is perpendicular polarization where the dipolar interaction is isotropic and repulsive. We also study Dy with a trapping potential of $(\omega_\rho,\omega_z){=}2\pi$ (10,1000) Hz. With $l_d = 400a_0$, this gives $g_d = 0.034$ in trap units. This is strongly interacting and to maintain the Kohn mode (center of mass slosh mode), we have used a low atom number, and for our example we use 300 atoms [22]. It is important to note that the Cr example is very similar to recent experiments [24]. In that work, they were able to vary $l_z/l_\rho$ between 0.1 and 0.17 and have up to 2000 atoms in a layer [24]. However, this is a layered system and interlayer dipolar interactions are important.

In contrast to a homogenous system, a trapped ideal 2D gas can have Bose condensation [3]. In this case, the critical temperature is at $T_{c0}/\hbar\omega = \sqrt{6N}/\pi \sim 0.78\sqrt{N}$. We will use this temperature to rescale our findings so that, to first order, we remove the number dependence of the results. This is important because, as we vary the temperature, we do not have exactly the same number of particles between every calculation. In the thermodynamic limit, the population of the condensate is $N_0/N = 1 - (T/T_{c0})^2$ [3].

For reference, we give several specific numerical examples in Table I. For two temperatures, we report $\mu$, $N_0/N$, $N$, and the Kohn mode energy (should be $1\hbar\omega_\rho$). For the Dy ($g_d = 0.034$) example, at $T/T_{c0} = 0.5$, the

TABLE I: Numerical examples of the HFBP for the q2D dipolar gas and contact gas.

| | $T/T_{c0}$ | $\mu/\hbar\omega$ | $N_0/N$ | $N$ | Kohn Mode/$\hbar\omega$ |
|---|---|---|---|---|---|
| $g_d$=0.0028 | 0.05 | 3.822 | 0.994 | 2004 | 0.9992 |
| | 0.5 | 3.457 | 0.658 | 1994 | 0.995 |
| $g_d$=0.0028 | 0.05 | 3.814 | 0.994 | 2004 | 0.9996 |
| $\tilde{X} = 0$ | 0.5 | 3.341 | 0.660 | 1994 | 0.997 |
| $g$=0.021 | 0.05 | 3.829 | 0.993 | 2004 | 0.9991 |
| | 0.5 | 3.541 | 0.662 | 1993 | 0.9995 |
| $g_d$=0.034 | 0.05 | 5.124 | 0.983 | 300 | 0.991 |
| | 0.5 | 4.919 | 0.525 | 298 | 0.976 |
| $g_d$=0.034 | 0.05 | 5.094 | 0.983 | 300 | 0.996 |
| $\tilde{X} = 0$ | 0.5 | 4.524 | 0.5500 | 303 | 0.987 |

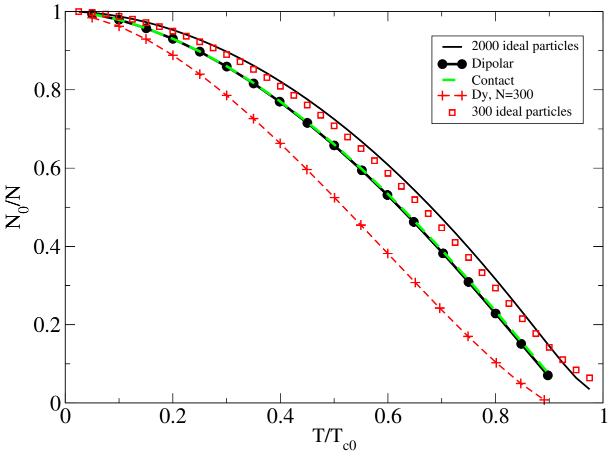

FIG. 1: (Color online) $N_0/N$ as a function of Temperature for the Cr dipolar gas (thick black line with circles), the contact gas (green dash dot), and for 2000 ideal trapped particles (solid black line). Additionally, a gas of 300 Dy particles (dashed red with +) and 300 ideal particles are shown (red open squares).

Kohn mode has noticably deviated from 1 by about 2.5%, this is about the worst the convergence of this mode gets as a function of temperature. For both dipolar examples, we show the results for when thermal exchange is negelected ($\tilde{X} = 0$). The lower temperature solutions are similar to the GPE solutions at $T = 0$.

## VI. PROPERTIES OF A Q2D DIPOLAR GAS AT FINITE TEMPERATURE

In this section we study the properties of a q2D dipolar gas at finite temperature, and compare it to a contact gas and a dipolar system without the thermal exchange. We look at several different aspects of these systems. First, we look at the condensate number as a function of temperature. Then, we compare the interaction contributions to the total energy. Third, we compare the density profiles of the contact and dipolar gas, at various temperatures. Fourth, we look at the impact of including the thermal exchange on the density profile of the gas. Finally, we look at the excitation spectrum as a function of temperature and total particle number. We also classify the lowest excitation modes.

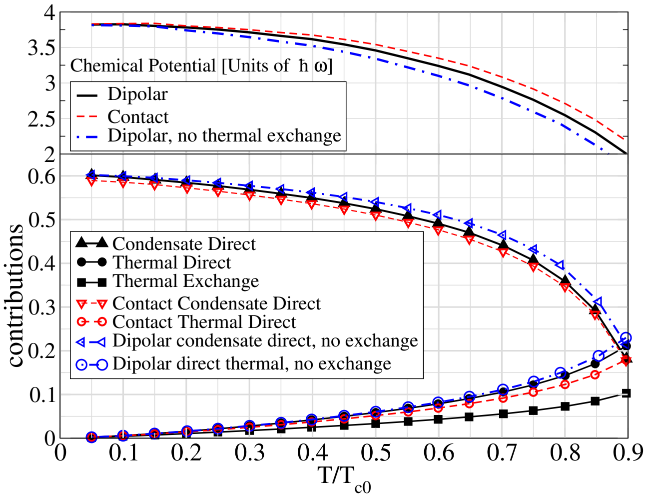

FIG. 2: (Color online) The chemical potential for three systems: dipolar (black), contact(dashed red), and dipolar without exchange (dash dot blue). The interaction terms for each system in the Hamiltonian as a function of temperature. The contributing terms are the direct condensate ($\langle\phi_0|D_0|\phi_0\rangle/\mu$, triangles), the direct thermal ($\langle\phi_0|\tilde{D}|\phi_0\rangle/\mu$, circles), and the thermal exchange ($\langle\phi_0|\tilde{X}/|\phi_0\rangle/\mu$, squares) interaction.

Figure 1 shows the condensate fraction for the Cr dipolar gas (black line with circles), the contact gas (green dash dot line), for 2000 ideal particles (solid black line), 300 Dy particles (dashed red), and 300 ideal particles (red open squares). The condensate fraction for the dipolar gas and contact gas are shifted down from the ideal gas (black line), with the dipolar gas being slightly lower than the contact gas. For the Dy example, it is clear that the interaction strongly depletes the condensate mode.

In Fig. 2 we look at the chemical potential and its contributions from Eq. 1, as a function of temperature. The examples shown are dipolar (black), contact (red), and dipolar without thermal exchange (blue). We show the direct condensate interaction ($\langle\phi_0|D_0|\phi_0\rangle/\mu$, triangle), the direct thermal interaction ($\langle\phi_0|\tilde{D}|\phi_0\rangle/\mu$, circle), and the thermal exchange interaction ($\langle\phi_0|\tilde{X}/|\phi_0\rangle/\mu$, square). For the contact interaction, the thermal exchange is equal to thermal direct interaction, so we only show one. For each example, the remaining contribution to the chemical potential is from $H_0$ or the potential and kinetic energy contributions.

For the dipolar gas, the thermal exchange term is about half as strong the direct contribution. The importance of the interaction with the thermal particles is more important as the temperature is increased. Comparing the dipolar calculation with and without the thermal exchange, we see that the chemical potentials agree reasonably well, the full calculation has a larger $\mu$ at high temperature. Looking at the interaction contributions, we see that the direct condensate (black triangle) and thermal interaction (black circles) make up a smaller portion of the chemical potential for the full calculation than the one with $\tilde{X} = 0$ (blue triangle and open circles).

In Fig. 3 we show both the total (black) and condensate density (red) for (a) a Cr system of 2000 particles and an analogous (b) contact system (near equal chemical potentials). We then compare the total density profiles in (c). The total density is in blue (black) for the dipolar (contact) systems, and the condensate density is shown in red. The temperatures from top to bottom are $T/T_{c0} = 0.25$ (dashed), 0.55 (dotted), 0.75 (dash-dot), and 0.90 (solid). For both the contact and dipolar gas at large $\rho$, the thermal density behaves as the analytic solution predicts.

An important point is that the dipolar gas has a higher density in the middle of the trap than the contact gas. It is hard to see in the figure, but the contact condensate atoms have been shifted to the shoulders of the condensate or near the trap edge. This has implications for the temperature at which the superfluid phase transition will occur in a dipolar gas.

In Fig. 4 we compare both the total and condensate density with and without the thermal exchange. We look at four temperatures, from top to bottom they are: $T/T_{c0} = 0.25$ (dashed), 0.55 (dotted), 0.75 (dash-dot), and 0.90 (solid). In 4 (a), a Cr gas with (blue) and without (black) the thermal exchange is shown. Additionally, the corresponding condensate density is with (red) and without (green) thermal exchange. This example with the thermal exchange is the same as Fig. 3 (a). In4 (b) a Dy gas with (blue) and without (black) the thermal exchange is shown. The corresponding condensate density is shown with (red) and without (green) thermal exchange. 4 (c) Shows a comparison of Dy and Cr with a large number of atoms (3700), when the chemical potentials are nearly the same at zero temperature. The densities are normalized to the maximum density at zero temperature.

In 4 (a) the impact of the thermal exchange is not too pronounced. It slightly increases the condensate central density, which is most obvious at high temperature. This is significantly different from the Dy example shown in 4 (b). There is a noticeable difference between the density profiles with and without the thermal exchange. The effect is most clearly seen in the condensate by looking at the increased central density and reduced extent of the red curve (with) versus green (without). At the highest temperature, where the validity of HFBP is questionable, we see a significant reduction in the condensate density and occupation. In fact the condensate repels the thermal cloud so strongly, that in the center of the trap there is a local minimum in the total density. Furthermore, the thermal exchange has significantly lowered the condenstate occupation. Thus the inclusion of the thermal exchange clearly lowers the critical temperature of the dipolar gas.

In 4 (c) we show that by varying $g_d$ and $N$ while holding $Ng_d$ constant, the HFBP does not give identical results as the $T = 0$ GPE would. For $g_d = 0.034, N = 300$ (Dy, black) and $g_d = 0.0028, N = 3700$ (Cr, blue) at low temperatures the density profiles are slightly different. More importantly, at high temperature the profiles are very different, this has to do with the strong depletion of the condensate.

In Fig. 5 we show the excitation spectrum of the dipolar gas (blue circles), a dipolar gas without the thermal exchange (red triangle), and the contact gas (black +) as a function of temperature. We have also characterized the excitations by their azimuthal symmetry. In a 2D contact gas, there is a hidden symmetry which makes the breathing mode ($m$=0) have an energy of $2\hbar\omega$ [38]. This mode has very little temperature dependence. This hidden symmetry is removed by the dipolar interaction, however if $l_z$ goes to zero, the breathing mode goes to $2\hbar\omega$. In the example we have picked ($g_d = 0.0028$ and $N$=2000), the $|m| = 3$ mode is near $2\hbar\omega$, but this is not the breathing mode ($m = 0$). Rather, the mode just below this, is the breathing mode. The contact gas excitation spectrum (black +) agrees well with Ref. [39]. They used $g \sim 0.002$ which accounts for the differences. It is a general feature that the dipolar gas has lower excitation energies than the contact gas. In Ref. [27], the 3D excitation spectrum as a function of temperature showed that for an oblate geometry the dipolar excitations are lower than the contact system. It is worth pointing, out that the dipolar calculations with and without the thermal exchange, agree well at low temperature. As the temperature is increased there is some disagreement between the two (blue circle and red triangle), but mostly for more highly excitated modes. The calculations without the exchange become higher in energy.

The modes that have strong temperature dependence are those with higher azimuthal symmetry. In contrast, the full bodied modes (large central amplitude) have a more constant excitation frequency as temperature is varied. The reason for this is discussed below.

In Fig. 6 we show the excitation spectrum as a function of $N$ for the dipolar (blue circles) at $T/T_{c0} = 0.05$. The plots on the right are contour plots of the quasi-particle modes ($u_\alpha$) for $N = 5000$ dipolar atoms. The contour lines are in 0.25 increments of the maximum value of $u_\alpha$ (i.e., 0.75, 0.5, ...,-0.75). Additionally, the negative regions are shaded blue. The condensate density contours are shown as a dashed black lines. The azimuthal symmetries are:(a) $m$=2 quadruple mode, (b) $m$=3, (c) $m$=0, breathing mode, (d) $m$=4, (e) $m$=1, and (g) $m$=5. We have shown one of the two degenerate modes ($\pm m$) at each energy when $m \neq 0$. If the contact system were plotted, we would see that excitations are always higher in energy for all $N$ shown.

The modes that are not strongly dependent on number or temperature are the modes that have a full bodied mo-

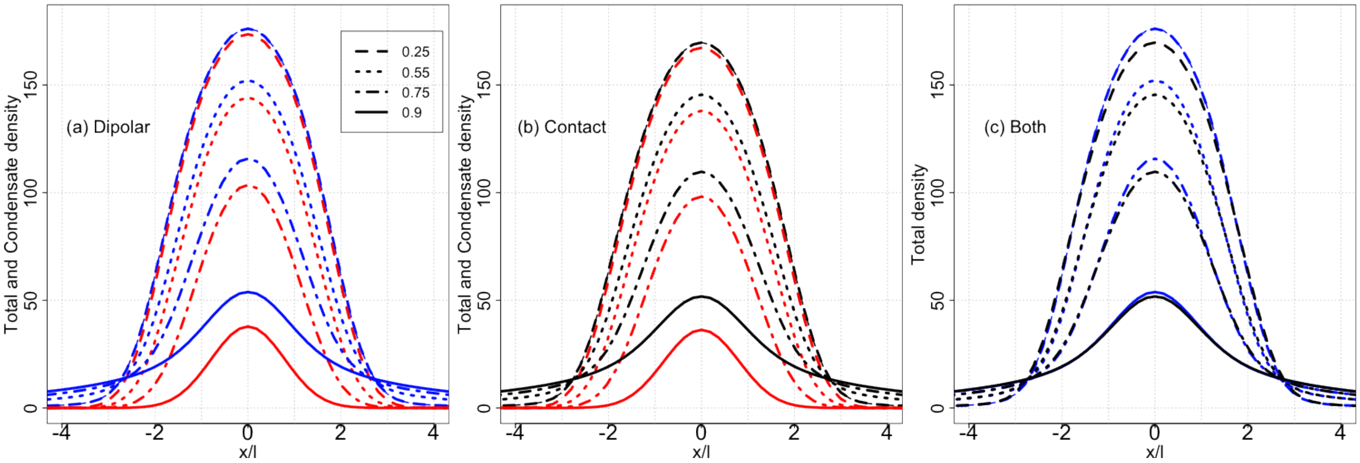

FIG. 3: (Color online) The total and condensate density of (a) a Cr dipolar gas and (b) contact gas, and the comparison of the total densities (c). The total density is in blue (black) for the dipolar (contact) gas, and the condensate density is in red. The temperatures from top to bottom are $T/T_{c0} = 0.25$ (dashed), 0.55 (dotted), 0.75 (dash-dot), and 0.90 (solid). (c) The dipolar gas is more dense in the center of the trap at all temperatures.

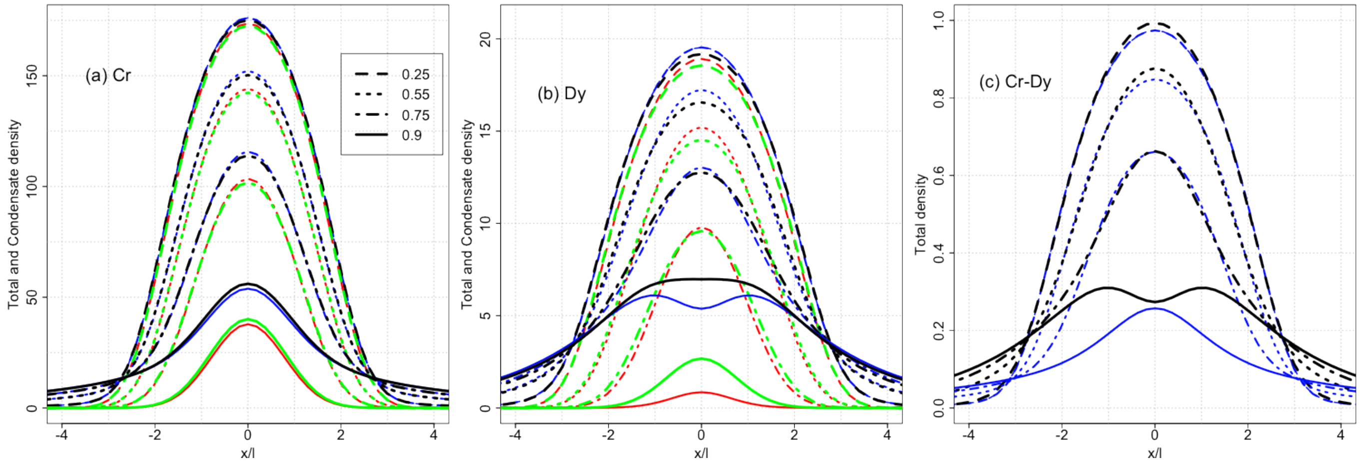

FIG. 4: (Color online) Comparison of density with and without thermal exchange. Both the total and condensate density are shown at four temperatures, top to bottom: $T/T_{c0} = 0.25$ (dashed), 0.55 (dotted), 0.75 (dash-dot), and 0.90 (solid). (a) A Cr gas with (blue) and without (black) the thermal exchange; the corresponding condensate density is with (red) and without (green) thermal exchange is shown. (b) For a Dy gas, the total density with (blue) and without (black) the thermal exchange; the corresponding condensate density with (red) and without (green) thermal exchange is shown. Both the condensate and total density without thermal exchange have a lower central density. (c) Shows a comparison of Dy (black) and Cr (blue) with a large number of atoms (3700) when the chemical potential are the same at zero temperature.

tion or large amplitude in the middle of the condensate, see Fig. 6 (c) and (e). These modes are mildly impacted by the total number of atoms in the system. The modes with higher azimuthal symmetries are more like surface modes, and are strongly effected by the number or temperature, see Fig. 6 (a), (b), (d), and (f).

In fact the strong number dependence leads to excitations crossing paths as $N$ is increased. The $m$=3, (b), mode becomes lower than the breathing mode, (c); and $m$=4, (d), mode becomes lower than the $m$=1, (e). The fact that surface modes move relative to full body excitations as a function of $N$ is related to the size of the condensate. Both as the atom number is increased, and as the temperature is decreased, the size of the condensate becomes larger. Naively, one might consider the surface of the condensate a ring with a restorating force. We consider the surface excitations as displacements of the ring from equilibrium, and find an excitation spectrum which behaves as $m/R$ where $R$ is radius of the ring [40]. Then we look at $m$ over the radius at which the density equals $0.25n_0(0)$ (the furthest out contour of the condensate in Fig. 6), we find a similar number dependence to the excitation spectra in Fig. 6. This is too simplistic, but gives a physical reason for such behavior in the excitation spectrum. The important point of this analysis is that the size of the condensate grows quickly at small $N$

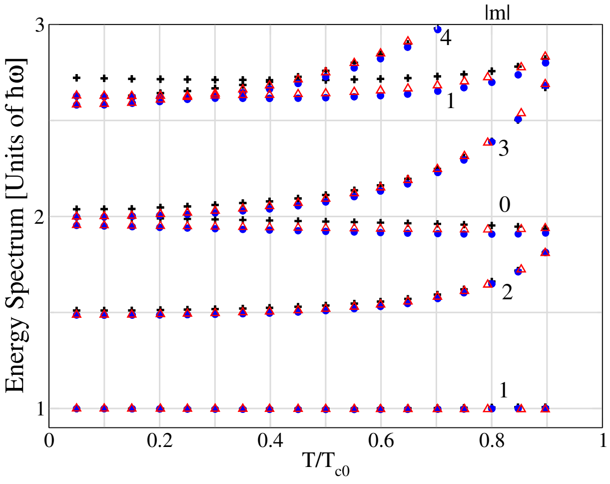

FIG. 5: (Color online) The excitation spectrum of the dipolar (blue circles), dipolar without exchange (red triangle), and contact gas (black +) as a function of temperature for $N = 2000$. The azimuthal symmetry of the excitations are shown next to each curve.

and slows down at larger $N$. Thus we see a rapid change in the excitation spectrum at low $N$ and less so at large $N$.

## VII. CONCLUSION

This paper studied a trapped q2D dipolar gases at finite temperature. We presented the numerical method used to solve Hartree Fock Bogoliubov Popov equations for a gas with non-local interactions including thermal exchange effects. It is worth noting that the thermal tail of this gas has of the standard form of a 2D gas and could therefore be used for accurate thermometry [2, 7]. This is not surprising, but still worth noting for experiments and using as a convergence test for theory.

In Fig. 1 we showed condensate fraction as a function of temperature for both the Cr and Dy examples. The critical temperature of the Dy is greatly reduced by the interactions. In Fig. 2 we looked at the chemical potential and the total interaction energy as a function of temperature for the various terms in Eq. 1. We compared the contact example with the Cr example with and without thermal exchange. In Fig. 3 we studied the impact of temperature on the density profiles and saw that the dipolar gas is more dense in the center of the trap.

Next in Fig. 4 we explored the impact of the thermal exchange on both the Cr and Dy examples. We found that the strongly interaction Dy example, the thermal exchange strongly reduces the condensate fraction at high temperature. This figure also presented a novel prediction of this study, when the dipolar interactions are strong and the temperature is near the transition temperature, the total density has a local minimum in the center of the trap where a small condensate strongly expels the thermal atoms. In Fig. 5 we studied the impact of temperature on the excitation spectra. We compared the contact example with the Cr examle with and without thermal exchange. Finally, in Fig. 6 we looked at the excitation spectrum of a Cr gas as a funciton of atom number and the quasi-particles, $u_\alpha$, for $N = 5000$. Here we illustrated the strong number or size dependence of the high azimuthal symmetries.

This work has set the stage to study phase coherence of a dipolar gas as a function of temperature, as has been done for contact gases [39]. We seek to understand how the non-local interaction will alter the correlations at the BKT transition. We already saw an increased phase space density in the middle of the cloud from the dipolar interaction. How does the dipolar interaction impact the phase coherence of the gas? Second, we wish to study roton physics in q2D [28, 41, 42]. In q2D, a roton can emerge as the field is tilted into the plane of motion, and leads to anisotropic density profiles [21]. The presented numerical method has been developed to handle this configuration.

This method could be applied to other momentum dependent interactions, for instance those with renormalized contact interactions, such as $g \to (g + g^2/k^2)$ [25]. Additionally, we could improve the scattering model to include more dipolar scattering physics [43].

### Acknowledgments

The author greatfully acknowledges support from the Advanced Simulation and Computing Program (ASC) and LANL which is operated by LANS, LLC for the NNSA of the U.S. DOE under Contract No. DE-AC52-06NA25396. The author is acknowledges enlightening discussions with L. A. Collins, R. M. Wilson, A. Sykes, and P. B. Blakie.

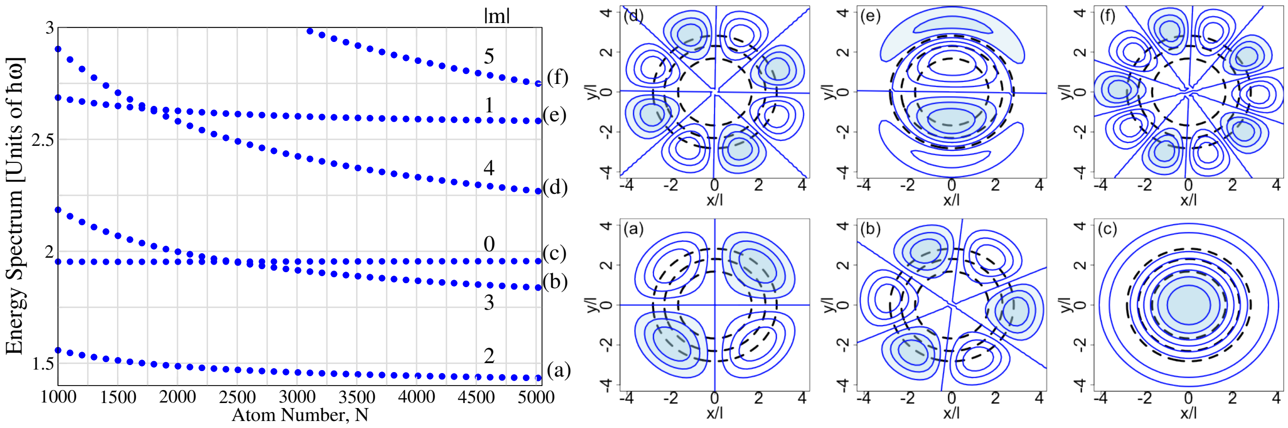

FIG. 6: (Color online) The excitation spectrum as a function of $N$ for the dipolar (blue circles) at $T/T_{c0} = 0.05$. The plots on the right are contour plots of the quasi-particle, $u_\alpha$, modes for $N = 5000$ dipolar atoms. The contour lines are are in 0.25 increments of the maximum value of $u_\alpha$ (i.e., 0.75, 0.5, ...,-0.75). Additionally, the negative regions are shaded blue. The condensate density contours (dashed black) are on the same scale.

---

[1] Berezinskii, V. L. Sov. Phys. JETP **34**, 610 (1972). L. M. Kosterlitz, D. J. Thouless, J. Phys. C **6**, 1181 (1973);

[2] Z. Hadzibabic and J. Dilibard, Riv. Nuo. Cime., **34**, 389 (2011).

[3] V. Bagnato and D. Kleppner, Phys. Rev. A **44**, 7439 (1991).

[4] Z. Hadzibabic *et al.*, Nature **441**, 1118 (2006).

[5] S. Tung *et al.*, Phys. Rev. Lett. **105**, 230408 (2010).

[6] P. Claude *at al.* Phys. Rev. Lett. **102**, 170401 (2009).

[7] C.L. Hung *et al.*, Nature **470**, 236 (2011); N. Gemelke, X. Zhang, C.-L. Hung, and C. Chin, Nature **460**, 995 (2009).

[8] N. Prokofev, O. Ruebenacker, and B. Svistunov, Phys. Rev. Lett. **87**, 270402 (2001)

[9] N. Prokof'ev and B. Svistunov, Phys. Rev. A, **66**, 043608 (2002).

[10] Z. Hadzibabic *et al.*, New J. of Phys. **10**, 045006 (2008).

[11] M. Holzmann, M. Chevallier, and W. Krauth, Europhys. Lett. **82**, 30001 (2008).

[12] R. N. Bisset *et al.* Phys. Rev. A, **79**, 033626 (2009).

[13] T. P. Simula *et al.* Phys. Rev. A, **77**, 023618 (2008).

[14] C. J. Foster, P. B. Blakie, and M. J. Davis, Phys. Rev. A **81**, 023623 (2010)

[15] R. N. Bisset *et al.* Phys. Rev. A, **79**, 013602 (2009); R. N. Bisset *et al.* Phys. Rev. A, **79**, 033626 (2009).

[16] H. P. Buchler *at al.* Phys. Rev. Lett. **98**, 060404 (2007).

[17] A. Filinov *at al.* Phys. Rev. Lett. **105**, 070401 (2010).

[18] K. Nho and D. P. Landau , Phys. Rev. A **72**, 023615 (2005).

[19] P. Jain, F. Ciniti, and M. Bonginsegni, Phys. Rev. B **84**, 014534 (2011).

[20] R. Nath, P. Pedri, and L. Santos, Phys. Rev. Lett. **102**, 050401 (2009).

[21] C. Ticknor, R. M. Wilson, and J. L. Bohn, Phys. Rev. Lett. **106**, 065301 (2011).

[22] M. Lu, N. Q. Burdick, S. H. Youn and B. L. Lev, Phys. Rev. Lett. **107**, 109401 (2011).

[23] Th. Lahaye *et al.* Nature **448**, 672 (2007); Th. Lahaye *et al.* Nature Physics **4,** 218 (2008); Th. Lahaye *et al.* Phys. Rev. Lett **101**, 080401 (2008).

[24] S. Meuller *et al.*, Phys. Rev. A **84** 053601 (2011).

[25] A. L. Fetter and J. D. Waleck, *Quantum Theory of Many-Particle Systems*, (Dover, New York 2003).

[26] D.S. Jin *et al.*, Phys. Rev. Lett. **77**, 420 (1996); M. Edwards *et al.* Phys. Rev. Lett. 77, 16711674 (1996); D. A. W. Hutchinson *et al.* Phys. Rev. Lettt. **78** 1842 (1997); R. J. Dodd *et al.* Phys. Rev. A **75** R32 (1998).

[27] S. Ronen and J. L. Bohn, Phys. Rev. A, **76**, 043607 (2006); S. Ronen, D. C. E. Bortolotti, and J. L. Bohn, Phys. Rev. A. **74**, 013623 (2006).

[28] S. Ronen, D. C. E. Bortolotti, and J. L. Bohn, Phys. Rev. Lett. **98**, 030406 (2007).

[29] R. N. Bisset, D. Baillie, and P. B. Blakie, Phys. Rev. A **83**, 061602 (2011).

[30] A. Griffin, Phys. Rev. B, **53**, 9341 (1996).

[31] B. Esry, Phys. Rev. A **55**, 1147 (1997).

[32] Y. Castin and R. Dum, Phys. Rev. A **57** 3008 (1998); C. Mora and Y. Castin, Phys. Rev. A **67** 053615 (2003).

[33] S. A. Morgan Phys. Rev. A **69** 023609 (2004).

[34] Uwe R. Fischer, Phys. Rev. A 73, 031602(R) (2006).

[35] P. B. Blakie *et al.* Phys. Rev. E, **80**, 016703 (2009).

[36] J. Reidl *et al.* Phys. Rev. A **59**, 3816 (1999).

[37] T. Bergman *et al.* Phys. Rev. A, **61**, 063605 (2000).

[38] L. P. Pitaevskii and A. Rosch, Phys. Rev. A **55** R853 (1997).

[39] C. Gies and D. A. W. Hutchinson, Phys. Rev. A, **70**, 043606 (2004); C. Gies et al., Phys. Rev. A, **69**, 023616 (2004).

[40] A. L. Fetter and J. D. Waleck, *Theoretical Mechanics of Particles and Continua*, (McGrall-Hill, New York 1980).

[41] R. Wilson, S. Ronen, and J.L. Bohn Phys. Rev. Lett. **104**, 094501 (2010).

[42] R. M. Wilson, S. Ronen, and J. L. Bohn, Phys. Rev. Lett. **100**, 245302 (2008).

[43] C. Ticknor, Phys. Rev. A **80**, 052702 (2009); Phys. Rev. A **81**, 042708 (2010); Phys. Rev. A **84**, 032702 (2011).